

# The contribution of the micro-turbulent velocity on the modelling of chromospheric lines in late type dwarfs\*

D. Jevremović<sup>1,2</sup>, J.G. Doyle<sup>1</sup>, and C.I. Short<sup>3</sup>

<sup>1</sup> Armagh Observatory, College Hill, Armagh BT61 9DG, N. Ireland (djc.jgd@star.arm.ac.uk)

<sup>2</sup> Belgrade Observatory, Volgina 7, 11160 Belgrade 74, Yugoslavia

<sup>3</sup> Department of Physics and Astronomy, University of Georgia, Athens, GA 30602-2451, USA

Received 29 October 1999 / Accepted 11 April 2000

**Abstract.** We discuss the influence of the non-thermal velocity (micro-turbulence) on the formation of chromospheric lines in the atmospheres of late type dwarfs. A review of previous work shows a variety of different approaches to the problem leading to different atmospheric structures and consequently different computed line profiles. In that light, we re-examine the formation of the Hydrogen Balmer lines and Na I D lines using twelve different distributions of the micro-turbulent velocity throughout the atmosphere. Our results show a wide range of possible line shapes. Using the analogy with the solar case and the latest results of the non-thermal component widths as derived from instruments on-board SOHO we model H $\alpha$  and the Na I D lines in an active dMe star Gl 616.2.

**Key words:** line: formation – line: profiles – turbulence – stars: activity – stars: chromospheres – stars: late-type

## 1. Introduction

Line widths of upper chromospheric and in particular transition region lines are broadened far in excess of their thermal widths. Over the last two decades there have been numerous measurements of line widths in the solar atmosphere (see references in Doyle et al. 1999) and with the advent of IUE and HST there exists measurements of high temperature transition region lines in many late-type stars (Linsky & Wood, 1994; Wood et al. 1996). The excess line width has been ascribed to micro-turbulence in the atmosphere on scale lengths of the photon mean free path in the atmosphere. With the launch of SOHO in 1995, the measurements of spectral line widths in different solar features, coronal holes, ‘quiet’ and active regions has been published (Teriaca et al. 1999, Doyle et al. 1999 and reference therein). The measured velocities range from 10 km s<sup>-1</sup> at a temperature of 10,000 K up to 30–35 km s<sup>-1</sup> at the top of the transition region.

With regard to the modelling of chromospheric lines there have been different approaches and approximations of the micro-turbulent/non-thermal velocity. The most important solar models are the ‘so called’ VAL models (Vernazza et al. 1976,

1981, Maltby et al. 1986). In their reference model, Maltby et al. (1986) used micro-turbulent velocities ranging from 1 km s<sup>-1</sup> in the photosphere, to 8.5 km s<sup>-1</sup> at a temperature of 8,000 K. For the cooler umbral model they varied the micro-turbulent velocity from zero to 4.1 km s<sup>-1</sup>.

Kelch et al. (1979) in modelling of atmospheres of late type stars used photospheric non-thermal velocities ranging from 2 km s<sup>-1</sup> to 5 km s<sup>-1</sup> in the upper layers. Giampapa et al. (1982) built a set of models for M dwarfs characterizing the non-thermal motions as isotropic Gaussian micro-turbulence and included the turbulent pressure in the hydrostatic equilibrium equation. They followed the treatment of micro-turbulent velocity by Kelch et al. (1979) with somewhat lower values up to 2 km s<sup>-1</sup>. Eriksson et al. (1983) produced a model for the late type star  $\beta$  Ceti (G9.5 III). Although the effective gravity in this star is much lower (log g=2.9) than in M dwarfs it is important to mention their treatment of the micro-turbulent velocity because it influenced some later work on late type dwarfs (e.g Short & Doyle 1998). They considered two models for the micro-turbulence. The first of their models equated the micro-turbulent velocity with the local sound speed. In the other model they kept the micro-turbulent velocity at a level of 2 km s<sup>-1</sup> up to the temperature minimum, then linearly increased it (in logarithm column mass) to 10 km s<sup>-1</sup> and kept this level throughout the remainder of the atmosphere.

Thatcher et al. (1991) modelled the K2V star  $\epsilon$  Eridani, linearly increasing the micro-turbulent velocity from 1 km s<sup>-1</sup> at the deepest photospheric levels to 5 km s<sup>-1</sup> at 300,000 K (i.e. the top of their atmosphere). Houdebine et al. (1995) produced an extensive grid of chromospheric structures using a value of 1 km s<sup>-1</sup> for the photospheric micro-turbulence. In the chromosphere they increased the micro-turbulent velocity to 2.5 km s<sup>-1</sup> at 8,200 K and in the transition region sharply increase it to 4.6 km s<sup>-1</sup>. Mauas & Falchi (1996) build models for the quiescent and flare state of the very active star AD Leo (M4.5Ve) using a very low micro-turbulent velocity of only 2 km s<sup>-1</sup>.

Short & Doyle (1998) built another grid of models and introduced the treatment of Eriksson et al. (1983) into the modelling of late type dwarfs. They use a constant micro-turbulent velocity in the photosphere of 2 km s<sup>-1</sup>, increasing it to 10 km s<sup>-1</sup> at the top of chromosphere and to 20 km s<sup>-1</sup> at the top of atmosphere.

Send offprint requests to: D. Jevremović

\* Based in part on observations made at Observatoire de Haute Provence (CNRS), France and SOHO

As is evident, differences in the approximation of the non-thermal velocities are significant. The most interesting point is that only Giampapa et al. (1982), Short & Doyle (1998) and Houdebine et al. (1995) were able to produce absorption in the case of the  $H\alpha$  line although Giampapa et al. (1982) considered the transition region at an unrealistic height, namely at column mass of  $\log m = -12$  (with  $m$  in  $\text{g cm}^{-2}$ ). Several of these latter works have shown the importance of the higher atmosphere (i.e. transition region) on the modelling of some chromospheric lines, however the question of what influence the micro-turbulence has on the formation of these lines has not been addressed properly.

The material in the following sections is organized as follows: in Sect. 2.1 we describe the basic models and some important details of the calculations. Sect. 2.2 describes in detail the different models of non-thermal velocity used, while in Sect. 3 we discuss our results. In Sect. 4 we discuss the results with reference to  $H\alpha$  and  $\text{Na I D}$  line observations of an active dMe star.

## 2. Construction of models and details of the calculations

### 2.1. Basic atmosphere

There exist two schools of thoughts for constructing ‘semi-empirical’ models of stellar atmospheres. One school follows a strict semi-empirical approach (VAL, Giampapa et al. 1982, Mauas & Falchi 1996) which means that they guess a starting solution for the atmosphere and then compare the output from the radiative transfer calculations to the observed spectral lines/fluxes. With the advent of faster computers there has emerged a new school which basically calculates grids of models (Houdebine & Doyle 1994, Short et al. 1997) by varying some of the important parameters in the atmosphere. After calculating the output of the models they compare the calculated results with observation and try to find which model gives the best agreement. We can call the latter approach ‘schematic’.

In order to investigate the different levels of the non-thermal velocities through the model atmosphere we kept the temperature structure versus column mass identical for all models. The temperature stratification is achieved using the ‘standard approach’, choosing the position of the temperature minimum and transition region. Up to the temperature minimum we keep the photospheric model as calculated in radiative equilibrium, from the temperature minimum to the top of the chromosphere we consider a linear temperature rise with the logarithm of the column mass and in the transition region we keep  $\log T$  versus  $\log m$  constant.

The photospheric model used is the ‘Next Generation’ model of Hauschildt et al. (1999) with the effective temperature of  $T_{eff} = 3800 \text{ K}$  and  $\log g = 5$  and solar metallicity. It is interesting that some authors use a lower effective gravity that we find to be of ‘historical’ origin – in the eighties the best photospheric models for late type stars were models of Mould (1976) which were between  $\log g = 4.75$  and  $5.75$ . We choose a photospheric model which corresponds to a dwarf star of spectral type M0-M1.

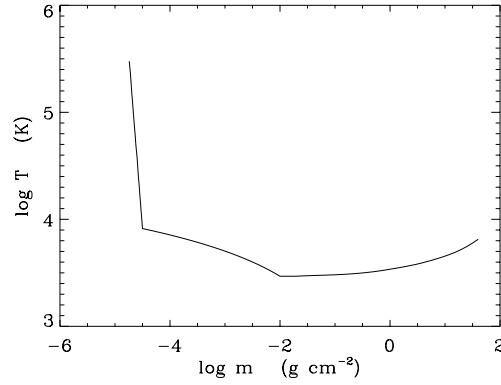


**Fig. 1.** The temperature dependence of the column mass for our test model.

From the temperature minimum, situated at  $\log m = -2$ , to the transition region, which onsets at temperatures around 8,200 K (Houdebine & Doyle 1994, Short & Doyle 1998) and in our test case at the column mass  $\log m = -4.5$ , we keep  $\frac{dT}{d\log m}$  constant. From the onset of the transition region to the top of the atmosphere at 300,000 K we keep  $\frac{d\log T}{d\log m} = -6.5$ . The temperature dependence on the column mass is shown in Fig. 1. Each atmospheric structure has one hundred depth points. This model is similar to the model used by Short et al. (1998) describing a so called zero-activity M dwarf.

### 2.2. Models for the non-thermal velocities

To test the influence of the non-thermal velocity on the electron density stratification and the line formation we use twelve different model distributions. These can be divided into three groups:

- A constant non-thermal velocity throughout the atmosphere for three different levels of  $v_{turb} = 1, 2$  and  $5 \text{ km s}^{-1}$ .
- Models where the non-thermal velocity depends on the sound velocity defined by

$$c_s^2 = \Gamma_1 \frac{p}{\rho} = \frac{\Gamma_1(1+x) * kT}{m_H} \quad (1)$$

where  $\Gamma_1$  is the generalized adiabatic exponent:

$$\Gamma_1 = \frac{\partial \ln p}{\partial \ln \rho} = \frac{5 + x(1-x) \left[ \frac{5}{2} + (\epsilon_H/kT) \right]^2}{3 + x(1-x) \left[ \frac{3}{2} + \left[ \frac{3}{2} + (\epsilon_H/kT) \right]^2 \right]}$$

(see e.g. Mihalas and Mihalas 1984, p.52).  $\epsilon_H$  is the ionization energy from the first level of the Hydrogen atom and  $x$  is the degree of ionization.

We consider five levels of the non-thermal velocity in the atmosphere namely  $0.1 c_s, 0.2 c_s, 0.5 c_s, 0.7 c_s$  and  $c_s$  and we limit the maximum non-thermal velocity to  $30 \text{ km s}^{-1}$ .

- Models where we keep the non-thermal velocity constant ( $1 \text{ km s}^{-1}$ ) up to the temperature minimum, then linearly increasing to (2, 3, 5 and  $10 \text{ km s}^{-1}$ ) at the top of the chromosphere and then to (5, 10, 20,  $30 \text{ km s}^{-1}$ ) at the top of the atmosphere.

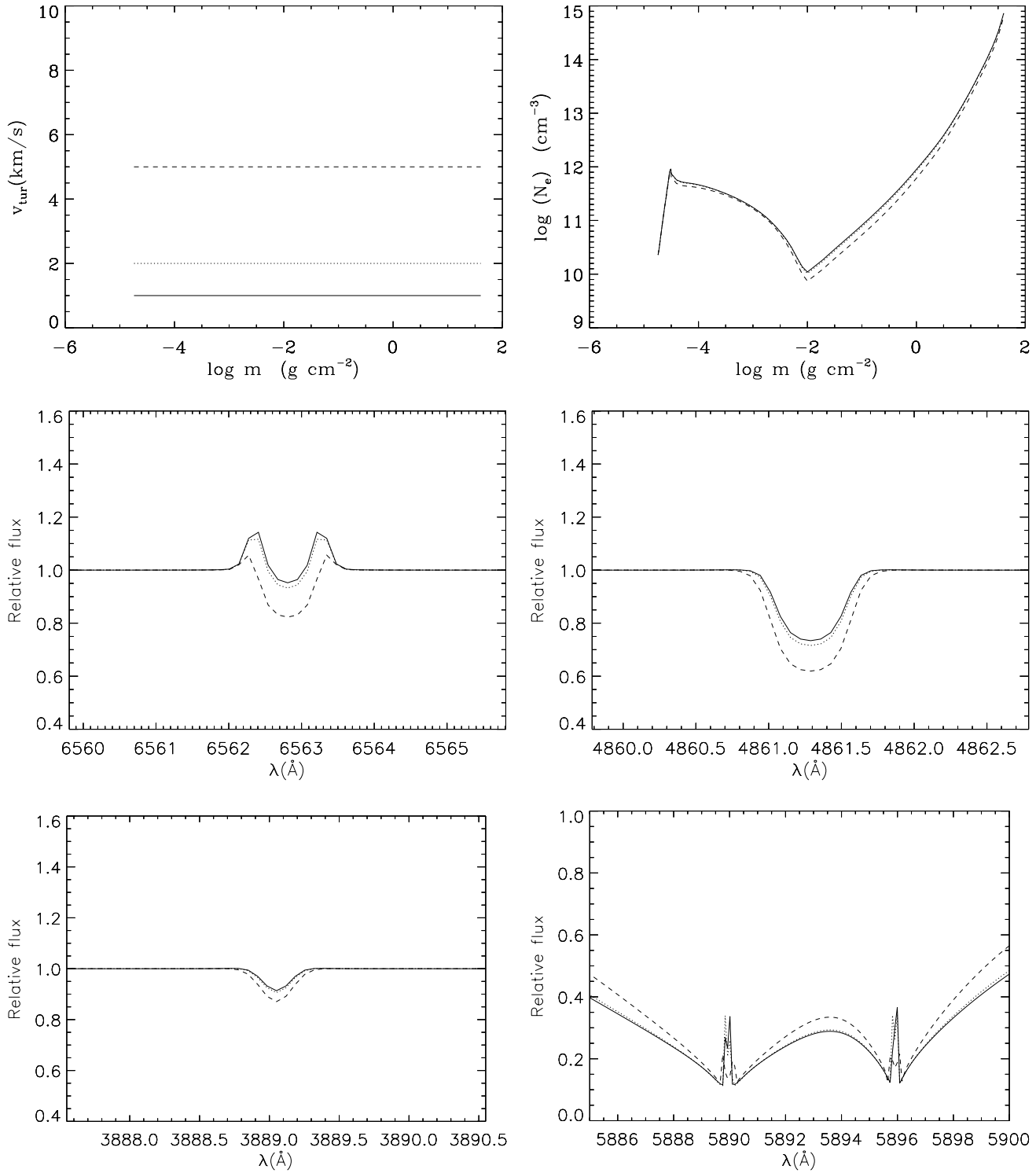


**Fig. 2.** The upper left panel shows models of constant non-thermal velocity. The upper right panel shows the final distribution of the electron density throughout the atmosphere while the middle panels show the line profiles of H $\alpha$ , H $\beta$  and the lower panels show the line profiles of H $\gamma$  and Na I D.

For the electron density calculation it is important to take into account turbulent pressure, therefore the hydrostatic equilibrium equation is written as:

$$g \times m = p_{\text{gas}} + p_e + p_{\text{rad}} + \frac{1}{2} \rho v_{\text{turb}}^2 \quad (2)$$

where  $g$  is the gravity acceleration,  $m$  the column mass,  $p_{\text{gas}}$ ,  $p_e$  and  $p_{\text{rad}}$  are the gas, electron and radiative pressure and  $\frac{1}{2} \rho v_{\text{turb}}^2$  is the turbulent pressure.

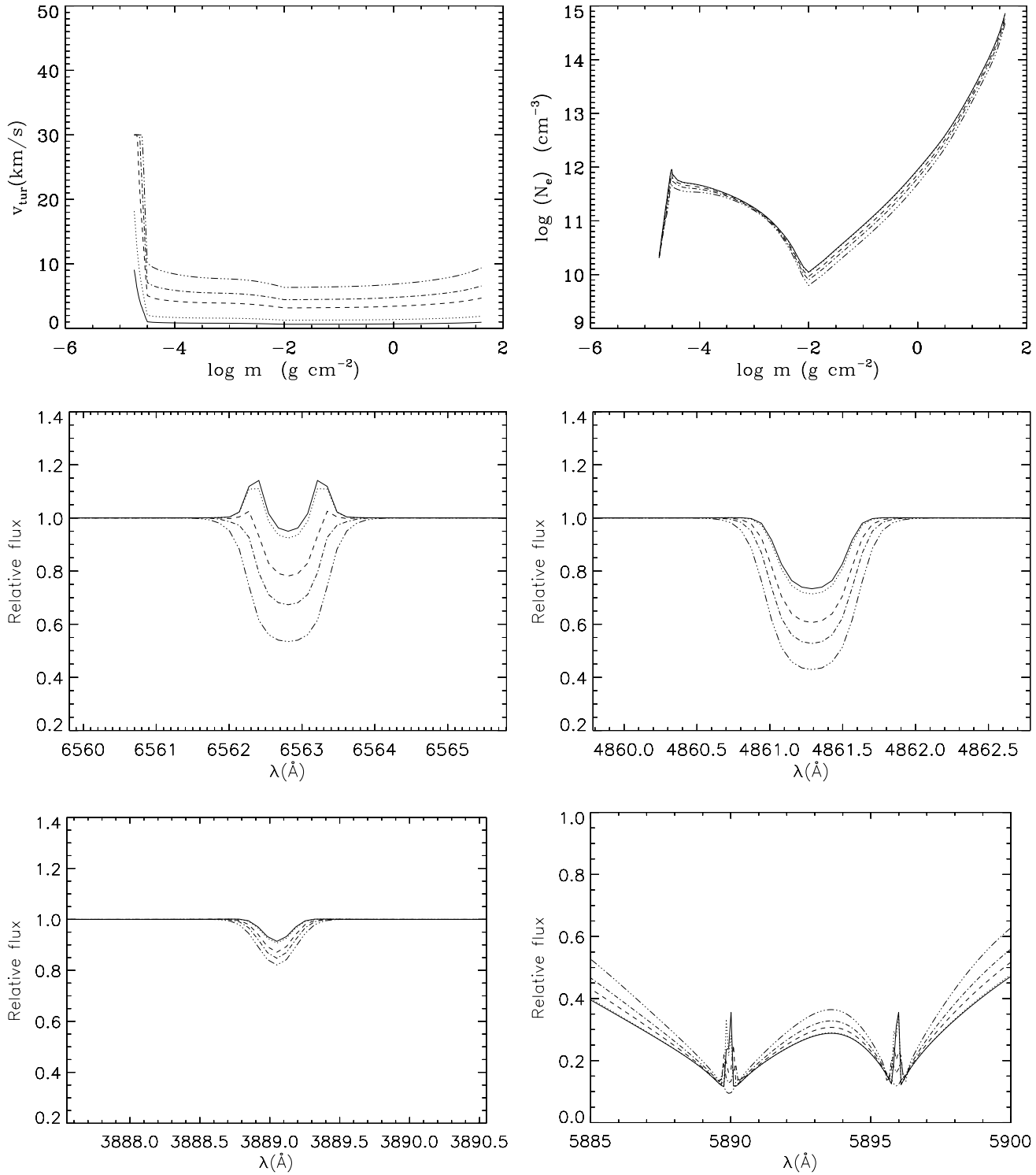


**Fig. 3.** Same as Fig. 2 except for the models of non-thermal velocity as a fraction of the sound speed. Solid line ( $0.1c_s$ ), dotted line ( $0.2c_s$ ), dashed line ( $0.5c_s$ ) and dot-dash line ( $0.7c_s$ ) and long dashed line ( $c_s$ ).

### 2.3. Details of calculation

We use the radiative transfer code MULTI (Carlsson 1986, 1992) to solve simultaneously the equations of radiative transfer, and the statistical and hydrostatic equilibrium equations for Hydrogen. Our Hydrogen model atom consists of 15 bound levels

plus continuum. The oscillator strengths were from Green et al. (1957), the transition probabilities from Reader et al. (1980) and the values for the Stark broadening from Sutton (1978). Our Sodium atom has 10 bound levels plus two continuum levels with the atomic data taken from Bashkin & Stoner (1982).

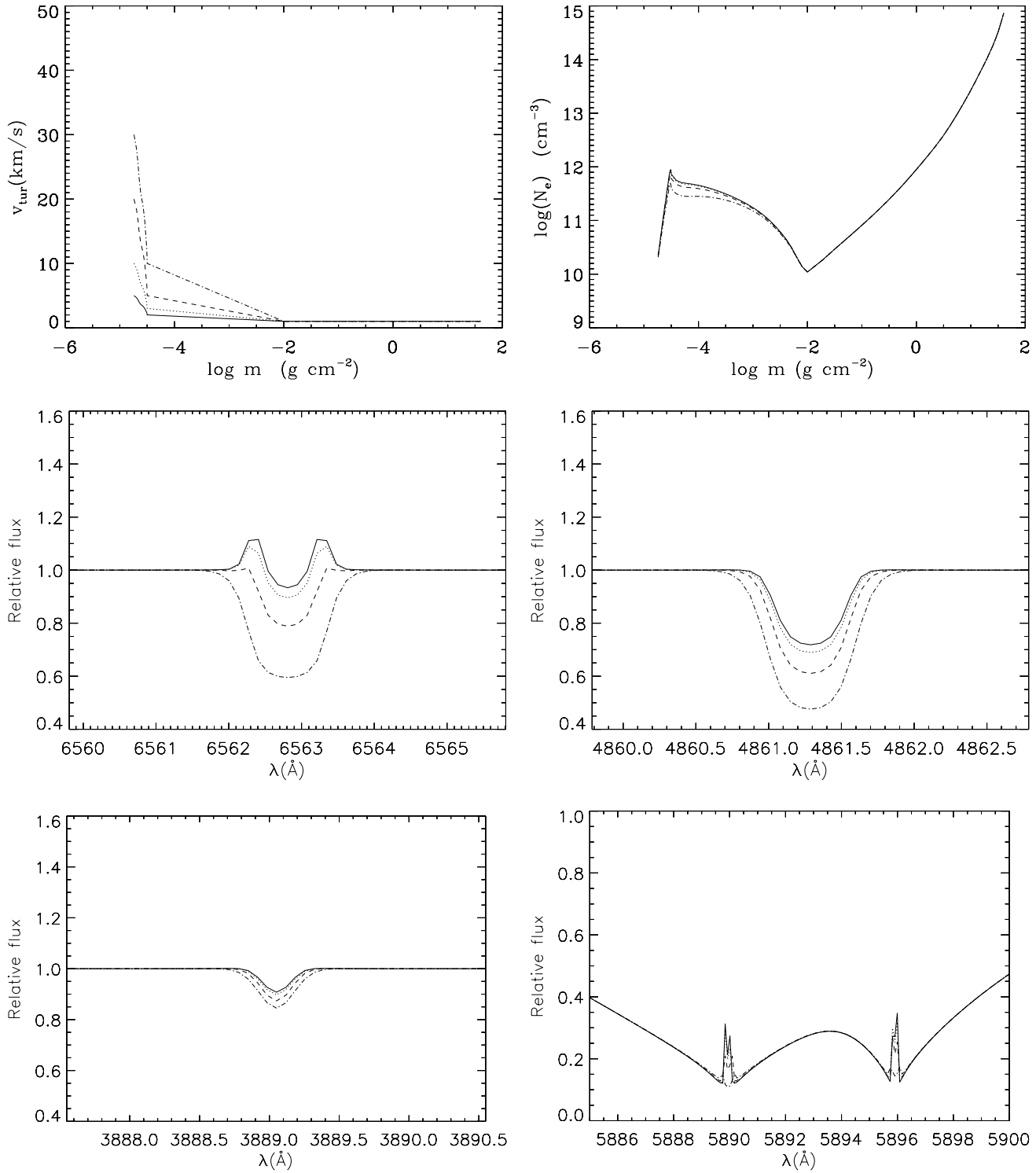


**Fig. 4.** Same as the Fig. 2 for the third type of non-thermal velocity distribution.

We use extensively the radiative-collisional switching technique of Hummer & Voels (1988) to achieve convergence of the population levels. The population of the levels in the Hydrogen and Sodium atom are iterated up to the level when changes are less than 1%.

In this calculation we have used opacities from the Uppsala opacity package. Andretta et al. (1997) and Short et al. (1997) have shown that it is necessary to include a better treatment of background opacities. At the moment we are working on the inclusion of a depth dependant micro-turbulent veloc-

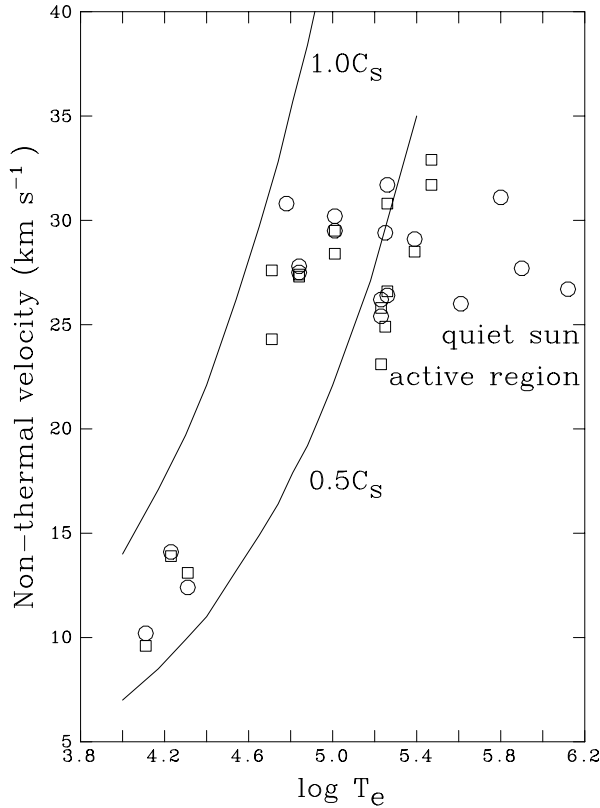


**Fig. 5.** The non-thermal velocity as determined by Teriaca et al. (1999) for an active region (squares) plus a ‘quiet’ sun region (circles). The lines corresponds to  $0.5c_s$  and  $c_s$ .

ity in PHOENIX. Thus to have a self-consistent treatment, we presently use only Uppsala opacities.

### 3. Results

In Figs. 2-4 we present the basic results of our calculations. The upper panels show the modelled non-thermal velocity distribution and the calculated electron density. The reminding panels show line profiles for four lines;  $H\alpha$ ,  $H\beta$ ,  $H\delta$  and  $Na\ I D$ .

#### 3.1. Constant velocity

From Fig. 2 we can see that there is a lowering of the electron density with increasing non-thermal velocity. Also, with the increase of non-thermal velocity, the  $H\alpha$  line shows a deeper self-reversal, while  $H\beta$  and  $H\delta$  change from emission to absorption.

In the Sodium doublet there are changes in the shape of the line wings with the lines becoming narrower with increasing non-thermal velocity. For turbulent velocities equal to or greater than  $5\text{ km s}^{-1}$ , the line wings change dramatically.

#### 3.2. Non-thermal velocity proportional to sound velocity

We can again see that the electron density is changed with changes in the level of the non-thermal velocity. By chang-

ing the non-thermal velocity from  $0.1c_s$  to  $c_s$  we manage to change the  $H\alpha$  profile from emission with the self-reversal to pure absorption.  $H\beta$  and  $H\delta$  both have a very small emission component even with a non-thermal velocity of  $0.1c_s$  and both lines again change their character similar to  $H\alpha$ .

The Sodium doublet again shows changes in the line shape. We attribute these changes to changes in the electron density in the photosphere. With an increase in the non-thermal velocity, the central emission in the lines weakens and in the case when the non-thermal velocity equal  $0.7c_s$ , almost completely disappears. There is a large increase in the intensity of the  $Na\ I$  wings with increasing turbulent velocity in the photosphere.

#### 3.3. Linearly increasing non-thermal velocity in the upper chromosphere

In the chromosphere/transition region, changes in the electron density are in agreement with Eq. (2). Again there are dramatic changes in the shape of the Balmer lines.  $H\alpha$  shows the most prominent changes – from emission in the case of a low non-thermal velocity to deep absorption with an increase in the level of the non-thermal velocity.

The wings of the Sodium doublet stay almost unchanged, which is easily explained by the constant non-thermal velocity in the photosphere. Again the emission core of the  $D$  line changes from being very prominent to almost non-existence with increasing non-thermal velocity in the chromosphere.

### 4. Comparison with the observations – the case of CR Dra

On May 21 1997, we obtained high resolution spectra of the active dM0e star Gl 616.2 (CR Dra) using the 1.9m telescope at the Observatoire de Haute Provence (OHP) and the fibre fed spectrograph ELODIE (Baranne et al. 1996). This spectrograph provides a spectral resolution of  $\frac{\lambda}{\Delta\lambda} = 45000$  throughout the visible part of the spectrum (between 3900 and 6700 Å). The OHP is situated at a relatively low altitude, and seeing is very rarely better than 2 arc sec (which is the diameter of the fibres).

We show in Fig. 5 the latest solar results based on measurements of both a ‘quiet’ Sun region and an active region, superimposed with curves for  $0.5c_s$  and  $c_s$ . These results would suggest that perhaps  $0.7c_s$  from  $10^4\text{ K}$  to  $10^5\text{ K}$  is an appropriate approximation while from 100,000 K to 300,000 K it is constant at  $\sim 30\text{ km s}^{-1}$ . For the lower photospheric region, we have used the results as derived in Sect. 2.2 which implies a level of  $\sim 5\text{ km s}^{-1}$  for the photospheric layers. As shown in Fig. 2, changes are only apparent in the line profiles for values of greater than or equal to  $5\text{ km s}^{-1}$ .

To compare our modelling results to the observations, we build a grid of models with the non-thermal velocity equal  $0.7c_s$ . In this grid of models we change the position of the transition region from  $\log m_{TR} = -4.8$  to  $-3.8$  and the position of the temperature minimum from  $\log m_0 = -2.5$  to  $-1.0$ . The comparison for  $H\alpha$  and  $Na\ I D$  lines are given in Fig. 6. We have normalized the fluxes to the continuum level at 5845 Å and 6540 Å for  $Na\ I D$  and  $H\alpha$  lines respectively. One can see that the Sodium doublet

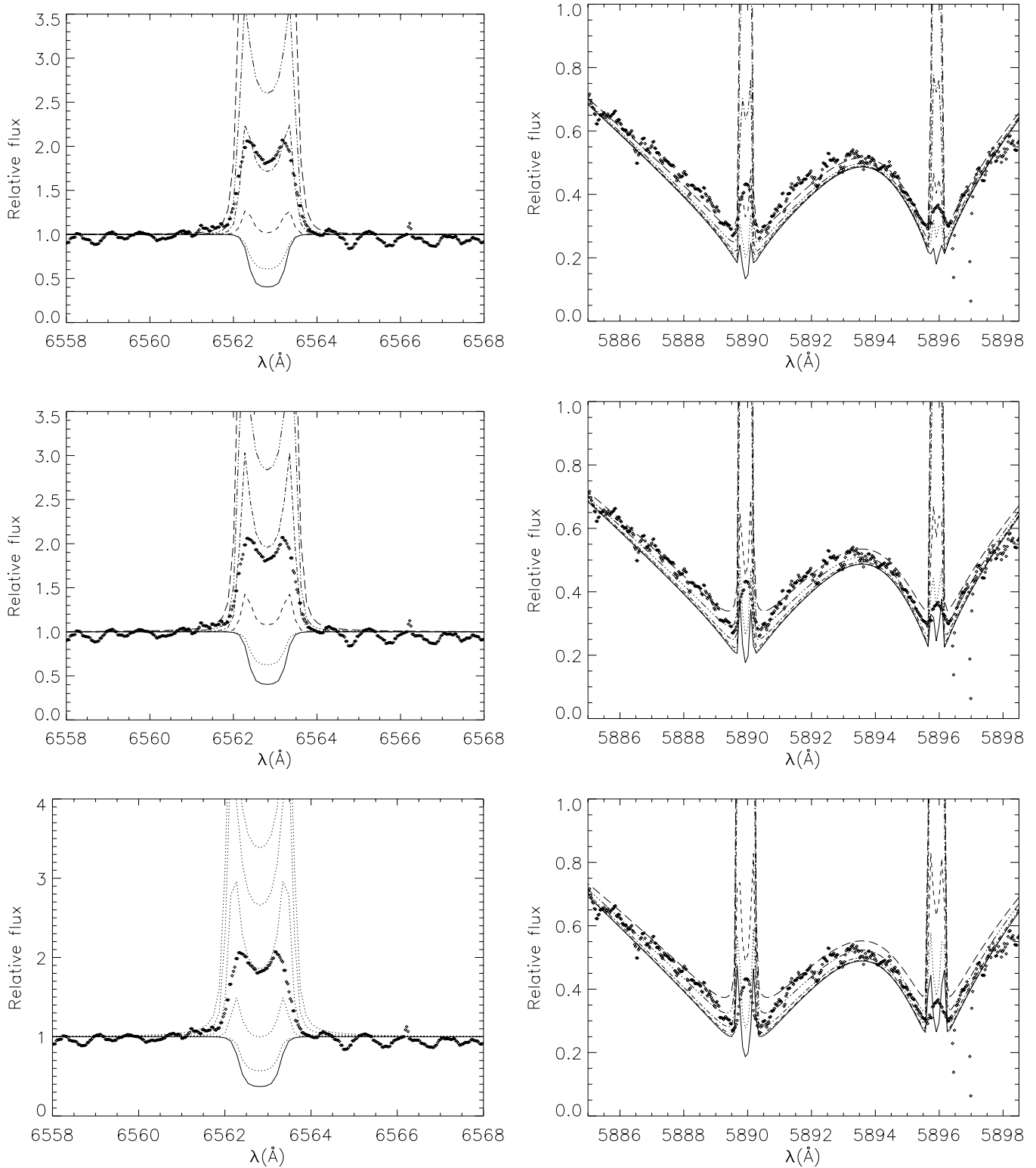


**Fig. 6.** The comparison between the observed and calculated fluxes in  $H\alpha$  (left panel) and Na I D lines (right panel) for CR Dra. The top panels show the case of  $\log m_0 = -2.0$ , middle panel for  $\log m_0 = -1.5$  and bottom panel  $\log m_0 = -1.0$ . The position of the transition region is as follows:  $\log T_{RM} = -4.8$  (solid line),  $-4.6$  (dotted line),  $-4.4$  (dashed line),  $-4.2$  (dot-dashed line),  $-4.0$  (dot-dot-dashed line) and  $-3.8$  (long dashed line).

is not fitted perfectly, especially in the wings. The main reason for this discrepancy is in the treatment of background opacities

(see Andretta et al. 1997). Additional opacities would lower the continuum level and consequently increase the relative fluxes.

The Sodium fits however suggest that the position of the temperature minimum is around  $\log m_0 = -1$ . Using that value we estimate from the  $H\alpha$  fits, that the transition region is at  $\log m_{TR} = -4.3$ . These values have to be confirmed with a better treatment of molecular opacities.

From the various fits one can see that the chosen value of  $0.7 c_s$ , which influences the width of the emission cores, agrees quite well with the observed ones for both  $H\alpha$  and  $Na\ I\ D$ .

## 5. Conclusions

Some earlier modelling, e.g. Houdebine et al. (1995) suggested that the level of micro-turbulence would not have an influence on the Hydrogen line profiles. This is clearly not the case as shown in the previous sets of figures. Of course one could argue that small scale motions with velocities close or even higher than the sound velocity are physically doubtful because of the generation of shocks. We think that in the light of new solar observations (SOHO) and the richness of small scale motions, we have to examine even these high levels of non-thermal velocities.

From the modelling it is clear that there is a lowering of the electron density with increasing turbulent velocity. Also, with increasing turbulent velocity,  $H\alpha$  shows a deeper self-reversal, while  $H\beta$  changes from emission to absorption. In  $Na\ I$ , there are changes in the shape of the line wings with the lines becoming narrower with increasing turbulent velocity, particularly for values greater than  $5\text{ km s}^{-1}$  in the photosphere.

Fairly good results were achieved for fitting the observed profiles of CR Dra. From our modelling we conclude that the model with transition region at  $\log m_{TR} = -4.3$  and a temperature minimum at  $\log m_0 = -1.0$  gives the best results for  $H\alpha$ , where  $Na\ I\ D$  is used to estimate the position of the temperature minimum.

*Acknowledgements.* Research at Armagh Observatory is grant aided by DENI while support for software and hardware is largely provided by the STARLINK Project which is funded by the UK PPARC. This work was supported by a grant (PPA/G/S/1997/00298) from the

UK PPARC. The Solar and Heliospheric Observatory is a project of international cooperation between ESA and NASA.

## References

- Andretta V., Doyle J.G., Byrne P.B., 1997, *A&A* 322, 266  
 Baranne A., Queloz D., Mayor M., et al., 1996, *A&AS* 119, 373  
 Bashkin S., Stoner Jr. J.O., 1982, *Atomic Energy-Levels and Grotrian Diagrams*. Vol. I, North Holl. Pub. Co.  
 Carlsson M., 1986, Uppsala Spec. Rept. No. 33  
 Carlsson M., 1992, In: Giampapa M.S., Bookbinder J.A. (eds.) *Cool stars. Proc. 7th Cambridge Workshop on Cool Stars, stellar systems, and the Sun*. ASP Conf. Ser. 26, p. 499  
 Doyle J.G., Teriaca L., Banerjee D., 1999, *A&A* 349, 956  
 Eriksson K., Linsky J.L., Simon T., 1983, *ApJ* 272, 665  
 Giampapa M.S., Worden S.P., Linsky J.L., 1982, *ApJ* 258, 740  
 Green L.C., Rush P.P., Chandler C.D., 1957, *ApJS* 3, 37  
 Hauschildt P.H., Allard F., Baron E., 1999, *ApJ* 512, 377  
 Houdebine E.R., Doyle J.G., 1994, *A&A* 289, 185  
 Houdebine E.R., Doyle J.G., Kościelicki M., 1995, *A&A* 294, 773  
 Hummer D., Voels S.A., 1988, *A&A* 192, 279  
 Kelch W.L., Worden S.P., Linsky J.L., 1979, *ApJ* 229, 700  
 Linsky J.L., Wood B.E., 1994, *ApJ* 430, 342  
 Maltby P., Avrett E.G., Carlsson M., et al., 1986, *ApJ* 306, 284  
 Mauas P.J.D., Falchi A., 1996, *A&A* 310, 245  
 Mihalas D., Mihalas B.W., 1984, *Foundations of Radiative Hydrodynamics*. Oxford University Press, New York – Oxford  
 Mould J.R., 1976, *A&A* 48, 443  
 Reader J., Corliss C.H., Wiese W.L., Martin G.A., 1980, *Wavelength Transition probabilities for Atoms and Atomic Ions*. NSRDS-NBS 68  
 Short C.I., Doyle J.G., Byrne P.B., 1997, *A&A* 324, 196  
 Short C.I., Doyle J.G., 1998, *A&A* 336, 613  
 Short C.I., Doyle J.G., Byrne P.B., Amado P.J., 1998, *A&A* 329, 229  
 Sutton K., 1978, *JQSRT* 20, 334  
 Teriaca L., Banerjee D., Doyle J.G., 1999, *A&A* 349, 636  
 Thatcher J.D., Robinson R.D., Rees D.E., 1991, *MNRAS* 250, 14  
 Vernazza J.E., Avrett E.G., Loeser R., 1976, *ApJS* 30, 1  
 Vernazza J.E., Avrett E.G., Loeser R., 1981, *ApJS* 45, 635  
 Wood B.E., Harper G.M., Linsky J.L., Dempsey R., 1996, *ApJ* 458, 761